Article:
MacKenzie, LE orcid.org/0000-0002-8151-0525, Choudhary, TR, McNaught, AI et al. (1 more author) (2016) In vivo oximetry of human bulbar conjunctival and episcleral microvasculature using snapshot multispectral imaging. Experimental Eye Research, 149. pp. 48-58. ISSN 0014-4835

https://doi.org/10.1016/j.exer.2016.06.008

In vivo oximetry of human bulbar conjunctival and episcleral microvasculature using snapshot multispectral imaging

L.E. MacKenzie,[1] T.R. Choudhary,[2,3] A.I. McNaught,[4,5] and A.R. Harvey.[1]

1. School of Physics and Astronomy, University of Glasgow, Glasgow, United Kingdom.
2. Institute of Biological Chemistry, Biophysics and Bioengineering, Heriot-Watt University, Edinburgh, United Kingdom.
3. EPSRC IRC "Hub" in Optical Molecular Sensing & Imaging, MRC Centre for Inflammation Research, Queen's Medical Research Institute, University of Edinburgh, Edinburgh, UK
4. Department of Ophthalmology, Cheltenham General Hospital, Gloucestershire Hospitals NHS Foundation Trust, Gloucestershire, United Kingdom.
5. Department of Health Professions, Plymouth University, Plymouth, United Kingdom.

Correspondence: Andrew Harvey, School of Physics & Astronomy, Kelvin Building, University of Glasgow, Glasgow, G12 8QQ, United Kingdom;
Andy.Harvey@glasgow.ac.uk

Abstract

Multispectral imaging (MSI) is now well established for non-invasive oximetry of retinal blood vessels, contributing to the understanding of a variety of conditions affecting the retinal circulation, including glaucoma, diabetes, vessel occlusion, and auto-regulation. We report the application of a unique snapshot MSI technique to enable the first oximetric imaging of the blood vessels of the anterior segment, i.e. the episcleral and bulbar conjunctival microvasculature. As well as providing a new capability of oximetry of the scleral vasculature, this technique represents ocular oximetry that is complimentary or alternative to retinal oximetry. We report the oxygen dynamics of these microvascular beds and assess how acute mild hypoxia effects the blood oxygen saturation (SO_2) of bulbar conjunctival and episcleral microvasculature.

A retinal-fundus camera fitted with a custom Image-Replicating Imaging Spectrometer enabled oximetric imaging of bulbar conjunctival and episcleral microvasculature in ten healthy human subjects at normoxia (21% Fraction of Inspired Oxygen [FiO_2]) and acute mild-hypoxia conditions (15% FiO_2). Eyelid closure was used to block oxygen diffusion between ambient air and the sclera surface. Four of the ten subjects – those that presented suitable vasculature for direct comparison between bulbar conjunctival and episcleral vessels - were imaged for 30 seconds following eyelid opening. Vessel diameter and Optical Density Ratio (ODR: a direct proxy for oxygen saturation) of vessels was computed automatically. Oximetry capability was validated using a simple phantom for the scleral vasculature,

Average episcleral diameter increased from 78.9 ± 8.7μm (mean ± standard deviation) at normoxia to 97.6 ± 14.3μm at hypoxia ($p = 0.02$). Diameters of bulbar conjunctival vessels showed no significant change from 80.1 ± 7.6μm at normoxia to

80.6 ± 7.0μm at hypoxia (p= 0.89). Acute mild hypoxia resulted in a decrease in SO_2 (i.e. an increase in ODR) from normoxia levels in both bulbar conjunctival (p <0.001) and episcleral vessels (p= 0.03).

Hypoxic bulbar conjunctival vasculature rapidly re-oxygenated in an exponential manner, reaching normoxia baseline levels, with an average ½ time to full reoxygenation of 3.4 ±1.4 seconds. This reoxygenation occurs because the bulbar conjunctival vessels are in direct contact with ambient air. This is the first study to characterise and also to image the oxygen dynamics of bulbar conjunctival and episcleral microvasculature, and to directly observe the rapid reoxygenation of hypoxic bulbar conjunctival vessels when exposed to air.

Oxygen diffusion into the bulbar conjunctiva must be taken into account to provide meaningful oximetry because bulbar conjunctival vessels will be highly oxygenated (close to 100% SO_2) when exposed to ambient air.

Oximetry of bulbar conjunctival vessels could potentially provide insight into conditions where oxygen dynamics of the microvasculature are not fully understood, such as diabetes, sickle-cell diseases, and dry-eye syndrome. Further, in vivo oximetry of individual capillaries and groups of flowing red blood cells could be achieved with a high magnification slit lamp adapted for MSI.

Keywords: multispectral imaging, oximetry, hypoxia, bulbar conjunctiva, episclera, oxygen saturation, microvasculature, oxygen diffusion,

1. Introduction

Multispectral imaging (MSI) is well established for non-contact oximetry of blood vessels (D J Mordant et al., 2011a; David J Mordant et al., 2011b) which has enhanced the understanding of a variety of retinal conditions, such as diabetes (Hammer et al., 2009; Hardarson and Stefánsson, 2012; Isenberg et al., 1986), glaucoma (Boeckaert et al., 2012; Mordant et al., 2014; Olafsdottir et al., 2011), and vessel occlusion (Eliasdottir et al., 2014), as well as auto-regulation response to flicker stimulation (Hammer et al., 2011) and acute mild hypoxia (Choudhary et al., 2013). However, oximetry of capillaries in the retina is beyond the technical capabilities of MSI-enabled retinal fundus cameras. The anterior segment provides two alternative ocular microvascular beds that are easily accessible for multispectral imaging and which could be used to probe ocular blood oxygen saturation and potentially provide new physiologically-relevant information; the bulbar conjunctival and episcleral microvascular beds. This is the first study to use MSI to non-invasively measure the oxygen saturation of bulbar conjunctival and episcleral microvasculature with high spatial and temporal resolution, revealing rapid oxygen diffusion from ambient air into bulbar conjunctival vessels.

The episcleral microvasculature is located within the scleral tissue, with few episcleral vessels visible near the scleral surface. In contrast, the bulbar conjunctival microvasculature is semi-mobile above the sclera, and presents many arterioles, venules, and capillaries for imaging (Meighan, 1956). Groups of individual red blood cells can be observed to flow in bulbar conjunctival capillaries if imaged with high magnification (Jiang et al., 2014). The bulbar conjunctiva may be unique in that it is the only microvascular bed in the human body which is directly exposed to ambient air. Figure 1a shows generalised vessel positions with respect to the sclera. Figure 1b shows a representative image of bulbar conjunctival and episcleral vasculature in

a single subject. However, despite potential for new oximetry information and ease of imaging, no MSI oximetry studies of either the bulbar conjunctival or episcleral microvasculature have been published to date.

MSI oximetry is based on the SO_2-dependent optical absorption spectra of haemoglobin. Changes in SO_2 can be calculated by imaging blood vessels at two wavelengths: one wavelength where optical absorption is sensitive to variations in SO_2, and at another wavelength which is insensitive to SO_2 variations (i.e. isobestic). From images of vessels, the optical density (OD) of vessels at each wavelength can be calculated, allowing the calculation of optical density ratio (ODR); ODR is directly proportional to SO_2. In vessels where SO_2 is known, ODR can then be empirically calibrated to SO_2 by assuming local arterial SO_2 is equal to the SO_2 of systemic arterial SO_2 as measured by pulse oximetry (Beach et al., 1999), or by using reference values from previous studies. (Hardarson et al., 2006).

To the best of our knowledge there are no reported MSI oximetry studies of the bulbar conjunctival or episcleral microvasculature. Instead, insights into the oxygen dynamics of microvasculature have generally been indirectly inferred from vessel-diameter or blood-flow measurements (Jiang et al., 2013; Shahidi et al., 2010; Wanek et al., 2013), however these parameters may be affected by factors other than changes in SO_2, such as conjunctival or episcleral inflammation. Direct measurement of the partial pressure of oxygen (pO_2) of the palpebral conjunctival microvasculature has been achieved with Clark-type electrodes (Chapman et al., 1986; Iguchi et al., 2005; Isenberg et al., 2002; Kwan and Fatt, 1971; Mader et al., 1987), however these electrodes have insufficient spatial discrimination for localisation of oximetry to blood vessels and crucially, block oxygen diffusion between ambient air and blood vessels under study.

In this study, we report the use of a retinal fundus camera modified for Snapshot Multispectral Imaging (SMSI) to non-invasively quantify the oxygen dynamics of both bulbar conjunctival and episcleral microvasculature in ten healthy human subjects. The high temporal resolution of the SMSI system (10ms exposure, 1Hz image acquisition rate) enables observation of fast biological processes (Fernandez Ramos et al., 2014). We observe rapid oxygen diffusion from ambient air into bulbar conjunctival vessels due to the unique location of the bulbar conjunctiva (i.e. directly in contact with ambient air); such observations are not possible with time-sequential MSI or Clarke-type electrodes because these techniques lack sufficient temporal and spatial resolution respectively.

2. Material and methods

2.1. Subject recruitment

This study was approved by the Ethics Committee of the University of Glasgow, College of Medical, Veterinary and Life Sciences. All volunteers provided written informed consent before participation and all procedures were performed in accordance with the tenets of the Declaration of Helsinki. Ten healthy volunteers (age 25 ± 2 years, six males and four female) were recruited. Subjects reported no history of ocular, respiratory, or vascular disease. Volunteers that regularly wore contact lenses or who were suffering from allergic conjunctivitis were excluded because this may induce fluctuating bulbar conjunctival vasodilatation (Gartner, 1944; Cheung et al., 2012; Jiang et al., 2014) .

2.2. Imaging system

The imaging system consisted of a commercial retinal fundus camera (Topcon TR50-DX; Topcon, Itabashi, Tokyo, Japan), fitted with an Image Replicating Imaging

Spectrometer (IRIS) and a cooled sCMOS camera (Zyla 5.5; Andor, Belfast, United Kingdom). IRIS is discussed in detail elsewhere (Harvey et al., 2005; Alabboud et al., 2007; Gorman et al., 2010; Fernandez Ramos et al., 2014); but in brief, IRIS simultaneously spectrally de-multiplexes a white-light image into eight distinct narrowband spectral images onto a single detector without rejection of light. Orthogonal-polarization imaging was used to minimise specular reflections from the sclera and blood vessels (van Zijderveld et al., 2014). Fundus-camera flash and image acquisition were synchronized using a custom graphical user interface written in LabVIEW, and images were saved in uncompressed Tiff format. Image acquisition was limited to 1Hz by the fundus camera flash refresh rate with an exposure time of 10ms. This imaging set-up and a representative multispectral IRIS image of the sclera are shown in Figure 2.

The curved scleral surface presents a challenge for imaging because it causes the position of blood vessels to vary with respect to the imaging plane of the fundus camera, potentially up to ~12mm from the anterior segment to the extreme lateral side of the sclera. To insure sharp focus over an extended scleral region, the 'small aperture' setting of the fundus camera was selected. This resulted in an estimated depth-of-field (DOF) of ~10mm; DOF was estimated by imaging a USAF test chart (USAF 1951 Chart; Applied Image Group-Imaging, Rochester, New York, USA) as it was moved through prime-focus on a linear-translation stage. A 35-degree field-of-view was selected to provide a field of view at the object plane of approximately 85 x 45mm. This combination of settings enabled the imaging of bulbar conjunctival and episcleral vessels over an extended scleral region with an optimal, sharp focus.

2.3. Scleral phantom

For assessment of the validity of our oximetry technique, a simple sclera-mimicking phantom was manufactured (see Figure 3). Similar phantoms have previously been used to validate retinal oximetry (David J Mordant et al., 2011). The phantom consisted of a transparent Fluorinated Ethylene Propylene (FEP) capillary of 100μm inner diameter (Zuess inc., Belfast, Northern Ireland), placed in contact with optical-grade Spectralon (Spectralon® Diffusion Material; Labsphere inc, North Sutten, New Hampshire, USA); Spectralon has similar spectral reflectance characteristics to the sclera (Bashkatov et al., 2010; Labsphere Inc.). To simulate in vivo blood circulation, ex vivo whole horse blood (40% hematocrit) (E&O labs, Bonnybridge, Scotland, United Kingdom) was flowed through the FEP capillary under feed from a syringe pump (KDS260, Linton Instrumentation, UK). SO_2 of the blood was reduced by adding measured quantities of Sodium Dithionite (EMD Millipore, Fisher Scientific, Loughborough, UK) to 5ml samples of blood according to the procedure described in Briely-Sabo and Bjornerud (Briley-Saebo and Bjornerud, 2000). SO_2 blood samples was measured prior to imaging using an optical blood gas analyser (GEM OPL, Instrumentation Laboratory, Bedford, Massachusetts, USA). A total of eight SO_2 samples ranging between 5% and 100% SO_2 were imaged in the FEP capillary.

2.4.1. Experimental procedure for in-vivo imaging

~~Subjects positioned their head in the standard fundus-camera chin-rest; head-straps were used to restrain the subject and minimise any motion. The fundus camera objective lens was positioned approximately five centimetres from the subject's sclera. In this configuration, the fundus camera illumination formed a circle approximately four centimetres in diameter. Subject gaze was controlled by the subject fixating on the fundus camera external fixation target (a movable red LED). For each subject, the scale of images was calibrated by imaging a millimeter scale located in the nominal plane of the sclera at prime focus. This yielded an average~~

~~image scale of 13.5 microns per pixel, enabling conversion of vessel diameter in pixels to diameter in microns.~~

Subjects positioned their head in the standard fundus-camera chin-rest; head-straps were used to restrain the subject and minimise any motion. The fundus camera objective lens was positioned approximately five centimetres from the subject's sclera. In this configuration, the fundus camera illumination formed a circle approximately four centimetres in diameter. Subject gaze was controlled by the subject fixating on the fundus camera external fixation target (a movable red LED). For each subject, the scale of images was determined by imaging a millimeter scale placed in front of the sclera at prime focus. All subsequent images were acquired at this focal position. This enabled a calibration of the size of each pixel on the detector to the real size of an image; on average, one pixel corresponded to ~13.5 microns. From this, the measured vessel diameter in pixels was calibrated to diameter in microns."

Scleral regions of each subject were selected for imaging so as to maximise the number of bulbar conjunctival vessels meeting the inclusion criteria (see Section 2.6.1). Bulbar conjunctival and episcleral vasculature was distinguished by moving the gaze of a subject; this moved the position of the bulbar conjunctiva above the sclera, altering the relative position of bulbar conjunctival and episcleral vessels. However it was not possible to classify individual vessels as arterioles and venules because of the diverse morphology of bulbar conjunctival vasculature and the limited number of episcleral vessels available for imaging (see Section 4.4). Scleral regions were chosen for imaging so as to maximise the number of bulbar conjunctival vessels meeting inclusion criteria whilst including some episcleral vessels for analysis (see Section 2.6.1). Once selected, the same blood vessels in a single

scleral region of a single eye for each subject were consistently imaged and analysed throughout the experiment.

Throughout the imaging protocol, the scleral region exposed to air was kept constant by the subject constantly gazing at the stationary fixation target and peripheral arterial SO_2 was recorded throughout the experiment using a fingertip pulse oximeter (AUTOCORR; Smiths Medical ASD Inc., Rockland, MA, USA) interfaced to a computer using a custom LabVIEW interface.

2.4.2. Repeatability

To assess repeatability of ODR measurement, eight consecutive images of the same scleral region were acquired in a period of approximately ten seconds for each subject**.** Gaze fixation was maintained for 2.5 minutes with their eyelid open prior to imaging to expose the target vasculature to ambient air.

2.4.3. Effect of eyelid closure

Eyelid closure was used to control oxygen diffusion; eyelid closure places a tissue barrier between the scleral surface and the ambient air, drastically decreasing the rate of any oxygen diffusion from ambient air to this scleral surface. To assess if eye closure affects the ODR of vessels, subjects were imaged before and after a period of eyelid closure. As before, subjects continually gazed at the fixation target for 2.5 minutes to expose the target vasculature to ambient air prior to imaging; subjects then closed their eyelids for a further 2.5 minutes. After 2.5 minutes of eyelid closure subjects opened their eyelid and synchronised imaging occurred

2.5.4. Acute mild hypoxia

To assess the effects of acute mild hypoxia on ODR, subjects were imaged at normoxia and acute mild-hypoxia. For normoxia measurement, subjects inhaled room air (21% FiO_2) for 2.5 minutes whilst fixating on the red LED fixation target, after which they were imaged. To induce acute mild hypoxia, subjects closed their eyelids and breathed a hypoxic air mixture (15% 2.5 minutes of inhalation of hypoxic air mixture (15% FiO_2) supplied via a hypoxic-air generator (Everest Summit II Hypoxic Generator; Hypoxico, Inc., New York, NY, USA) (Spurling et al., 2011). The hypoxic-air generator was calibrated before use and the air supply was monitored with an in-line oxygen analyzer (AD300 oxygen analyser; Teledyene Analytical Instruments, City of Industry, California, USA). Hypoxic air generators have been previously used for a study into retinal response to acute mild hypoxia (Choudhary et al., 2013).

After 2.5 minutes of hypoxic-air inhalation, subjects opened their eyelids and synchronised imaging occurred. Synchronisation of imaging with events, such as eyelid opening, was accomplished with a five-second oral countdown and with an accuracy of ±1 seconds. Subjects were then returned to normoxia by breathing room air. This process was repeated in the following sequence: normoxia 1, hypoxia 1, normoxia 2, hypoxia 2, normoxia 3; this sequence provides a robust time-sequential modulation in SO_2 and associated ODR change that is highly distinct from normal physiological variations.

2.5.5. Exposure of hypoxic vasculature to ambient air

A sub-group of four subjects (3 male, 1 female) were selected for further study. These subjects presented bulbar conjunctival and episcleral vessels suitable for analysis within single scleral region, allowing concurrent imaging - and thus comparison of oxygen dynamics - between bulbar conjunctival and episcleral

vessels. Hypoxia was induced as described in section 2.5.3. However, when subjects opened their eyelids, a synchronised 1Hz frame-rate imaging sequence was subsequently recorded for the 30 seconds, enabling observation of any rapid diffusion processes. This was repeated twice per subject.

2.6. Image analysis

2.6.1 Vessel section inclusion criteria

The following inclusion criteria were applied to ensure that only appropriate vessel sections were selected for analysis: (1) vessel sections had to be greater than 5 pixels (~67μm) in diameter to ensure that the contrast is not significantly affected by the modulation-transfer function of the imaging system. (2) vessel section had to have no other vessel sections within 12 pixels of either side of the vessel to be analysed; the presence of small vessels was accepted due to the high number of small bulbar conjunctival vessels; (3) vessel sections had to be at least 30 pixels long (~405μm); (4) vessels close to vessel intersections, regions of scleral glare, specular reflections, or images with poor focus were excluded; (5) episcleral vessels had to be of high apparent contrast with respect to the scleral tissue and not show a significant decrease in contrast along the analysed vessel section length (i.e. not appear to go deeper in the sclera tissue); (6) vessel sections had to meet all these inclusion criteria for all images in each section of the study.

2.6.2. Vessel tracking

Image processing was implemented post hoc using custom algorithms implemented in MATLAB. Raw IRIS images were cropped and co-registered to create a multispectral data cube. Vessels were tracked semi-automatically using manually identified control points. Repeated semi-automatic tracking demonstrated negligible variation in ODR (a standard deviation of <0.5% in 10 repeated measurements).

316 Fully automatic tracking was not implemented because inter-image registration of
317 bulbar conjunctival vessels is affected by the relative motion of bulbar conjunctival
318 and episcleral vasculature (Crihalmeanu and Ross, 2012).
319
320 **2.6.3. Oximetric analysis and vessel diameter measurement**
321 Our oximetric analysis is based on two-wavelength oximetry developed by Beach et
322 al (Beach et al., 1999). For two-wavelength oximetry, the optical-density (OD) of
323 blood vessels at two spectral wavebands is calculated: one waveband where optical
324 absorption is insensitive to changes in SO_2 (isobestic) and one waveband where
325 optical absorption is sensitive to changes in SO_2 (contrast). The 570nm IRIS
326 waveband was utilised as the isobestic reference and the 560nm waveband was
327 used as the oxygen sensitive waveband (Prahl, 1999). Each waveband has a full
328 spectral-width of approximately 7nm (Fernandez Ramos et al., 2014). Simple
329 modelling based upon the Beer-Lambert law of optical absorption shows that the OD
330 of blood vessels of ~60-100μm at 560nm and 570nm wavebands is expected to be
331 between 0.15 and 1; near-optimal for oximetry (van Assendelft, 1970).
332
333 A vessel-fitting algorithm was used to estimate vessel diameter (in pixels) and optical
334 transmission of vessels (see Figure 4). Vessel diameter at 570nm was estimated
335 according to the method described by Fischer et al.,(Fischer et al., 2010), where the
336 vessel boundaries are defined as the points in the vessel profile with the maximum
337 rate of change in grayscale intensity. This provided reputable fitting for both bulbar
338 conjunctival and episcleral vessels. Using this fitting algorithim, greyscale intensity in
339 the centre of each vessel (I_v) was calculated and the background greyscale intensity
340 at the centre of the vessel (I_o) was estimated by a linear fit to the background. OD
341 was then calculated for each wavelength by:

$$OD_\lambda = - \log_{10} \left(\frac{I_v}{I_o} \right). \quad (1)$$

ODR, defined as ODR = OD_{560}/OD_{570}, was then calculated for each vessel; ODR is a direct proxy for SO_2; if SO_2 increases, ODR decreases. ODR is approximately independent of vessel diameter and concentration of hemoglobin.

If two or more reference SO_2 values are known, then ODR can be empirically calibrated to SO_2 (Beach et al., 1999). However, no calibration is possible for this study because no empirical measurements of SO_2 in either bulbar conjunctival or episcleral vasculature have been reported in the literature, so we report results simply in terms of ODR.

3. RESULTS

3.1 Sclera phantom

A total of eight ex vivo blood samples of various oxygenations were imaged and analysed in the scleral phantom. Some variation in ODR was seen as blood flowed along the capillary. Overall, ODR was found to decrease with increasing SO_2 and the data was well fitted by a linear trend ($R^2 = 0.89$) (see Figure 5), validating the use of our MSI technique for oximetry of vessels in a scleral-like configuration. Repeatability of scleral phantom ODR measurements was <0.5% (standard deviation of 10 consecutive images).

3.2 Repeatability of in vivo ODR

The repeatability of in vivo ODR measurements is summarised in Table 1. The greater repeatability of ODR measurement of bulbar conjunctival vessels (0.96%) compared to episcleral vessels (1.55%) when calculated as an average across vessel type is probably due to the larger number of bulbar conjunctival vessel sections analyzed (57 in total) compared to episcleral vessel sections (22 in total); the larger number of vessels analysed reduces the sensitivity to fluctuations in ODR.

3.4. Eyelid closure during normoxia

Eyelid closure during normoxia resulted in no statistically significant change in ODR of either bulbar conjunctival or episcleral vessels. When the eyelid was open with constant gaze for 2.5 minutes, the average ODR was 0.90 ± 0.08 (mean ± standard deviation) for bulbar conjunctival vessels and 0.94 ± 0.09 for episcleral vessels. After eyelid closure, average ODR was 0.90 ± 0.08 for bulbar conjunctival vessels and 0.93 ± 0.08 for episcleral vessels ($p = 0.99$, 0.72 respectively; paired t-test).

3.5. Acute mild hypoxia

Table 2 and Figure 6 summarise measurements of ODR, vessel diameter, and fingertip pulse oximetry at normoxia and hypoxia. Figure 6a shows ODR and pulse oximeter data throughout the whole normoxia/hypoxia sequence. Bulbar conjunctival ODR increased with hypoxia (indicating a reduction in SO_2) from 0.846 ± 0.014 (mean ± standard error) at normoxia to 0.916 ± 0.011 at hypoxia ($p < 0.001$, paired t-test) (Figure 6b). Episcleral ODR increased on average, from 0.881 ± 0.019 (mean ± standard error) at normoxia to 0.938 ± 0.018 at hypoxia ($p = 0.03$, paired t-test) (Figure 6c). Figure 7 shows an overlaid ODR map of vessels at normoxia and hypoxia.

Bulbar conjunctival vessel diameter did not change significantly between normoxia and hypoxia ($p = 0.89$, paired t-test), however increases in vessel diameters were apparent in some subjects, whereas decreases in diameters were seen in others (Figure 6d). Diameters of episcleral vessels were observed to increase from 78.9 ± 8.65μm (mean ± standard deviation) at normoxia to 97.6 ± 1 4.3μm at hypoxia (Figure 6e) ($p = 0.02$, paired t-test).

3.6. Exposure of hypoxic vasculature to ambient air

For all eight datasets (four subjects, each imaged twice) ODR of hypoxic bulbar conjunctival vessels rapidly decreased upon eyelid opening (indicating an increase in SO_2), tending asymptotically to an ODR corresponding to ODR measured at normoxia. The variation in ODR was well-fitted by an exponential-decay function representing re-oxygenation of the conjunctival vessels plus a linear component, reflecting the incoming hypoxic blood supply:

$$OD = a * e^{-bt} + ct + d \quad (2)$$

Where t is time and a, b, c, d, are empirically calculated constants. The half-time to full reoxygenation ($T_{1/2}$) can then be calculated by:

$$T_{1/2} = -\frac{ln(2)}{b}. \quad (3)$$

$T_{1/2}$ varied on both an intra and inter-subject basis (see Table 3) but averaged over all measurements $T_{1/2}$ was 3.4 ± 1.4 seconds (mean ± standard deviation). Figure 8 shows this reoxygenation process in two representative subjects.

Episcleral vessel ODR remained higher (i.e. lower SO_2) after eyelid opening than at normoxia levels and was well fitted by a linear trend. Pulse oximeter SO_2 followed a similar trend to episcleral ODR.

4. Discussion

4.1. Validation of oximetry technique using scleral phantom

Results from the scleral phantom measurement validated the ability of the spectral imaging technique to characterise ODR for oximetry for blood vessels. Some variation in ODR was observed when blood flowed through the capillaries; this variation is likely to be due to non-homogenous SO_2 due to non-uniform deoxygenation by discrete crystals of Sodium Dithionite added to blood (Briley-Saebo and Bjornerud, 2000). Further variation in ODR may be caused by the

aggregation of blood cells, which alters the optical path of light through blood. Nevertheless, the results shown in Figure 5 clearly support that ODR decreases be with SO_2.

4.2. Effects of acute mild hypoxia

In episcleral vessels, vessel diameter increased and SO_2 decreased at acute mild hypoxia conditions. This is similar to auto-regulation of retinal vessels during acute mild hypoxia (Choudhary et al., 2013). In bulbar conjunctival vessels, SO_2 also decreased with hypoxia, but average vessel diameter did not change significantly. This confirms that the increase in ODR observed is due a decrease in SO_2 and not due a secondary effect due to change of vessel diameter.

4.3. Consequences of oxygen diffusion

Our study is the first to directly show that oxygen diffusion from air results in rapid reoxygenation and saturation of hypoxic bulbar conjunctival vessels. This measurement would not be possible with Clark electrodes, which are limited to a single point measurement and crucially, block oxygen diffusion between ambient air and the tissue in measurement. Hill and Fatt (1963) did however use a Clarke electrode to demonstrate that the bulbar conjunctiva would uptake oxygen from a limited pO_2 reservoir via diffusion, concluding that oxygen diffusion from ambient air to the exposed bulbar conjunctival vessels occurs constantly (Hill and Fatt, 1963). This study is the first to directly observe how this oxygen diffusion alters bulbar conjunctival SO_2.

It is expected that when in equilibrium with ambient air (pO_2 ~160mmHg), bulbar conjunctival vessels will be close to 100% SO_2 because normal arterial blood (~95-97% SO_2) corresponds to a typical pO2 of 80-100mmHg; much less than 160mmHg

448 (Verma and Roach, 2010; Williams, 1998). The average ODR was of exposed
449 bulbar conjunctival vessels was consistently ~0.95 (see Figure 6a), indicating a
450 constant equilibrium as expected.
451
452 In retinal oximetry, ODR is often empirically calibrated to SO_2 by assuming retinal
453 arterial SO_2 to be equal to the systemic arterial SO_2 as measured by a pulse
454 oximeter. Our results show that the oxygen dynamics of episcleral vessels are
455 similar to pulse oximetry, so this calibration approach would be valid for episcleral
456 vessels if arteries and veins could be accurately identified. However, this calibration
457 approach would not be valid for bulbar conjunctival vessels because our results
458 show that the oxygen dynamics of bulbar conjunctival vessels do not reflect the
459 oxygen dynamics of systemic arterial SO_2
460
461 **4.4. Challenges of bulbar conjunctival and episcleral oximetry**
462 In the retina, oximetry results are often reported independently for arterioles and
463 venules. However, in this study we report results for generalised vasculature and not
464 separately as arterioles and venules for several reasons. (1) Bulbar conjunctival
465 arterioles and venules could not be reliably distinguished from morphology alone due
466 to the significant variation in bulbar conjunctival vessel morphology (Meighan, 1956).
467 (2) Bulbar conjunctival vessels will be highly oxygenated when exposed to ambient
468 air due to oxygen diffusion from air, and thus could not be distinguished on the basis
469 of ODR. (3) The relatively low number of episcleral vessels that met inclusion criteria
470 did not allow sufficient comparison to identify arteries and veins by either vessel
471 morphology or ODR. Reliable discrimination between episcleral arteries and veins
472 could however be achieved with fluorescence angiography (Ormerod et al., 1995).
473

Rattlesnaking - a false apparent change in ODR along the length of a vessel section - is a common artefact in two-wavelength oximetry. Rattlesnaking was observed in both bulbar conjunctival and episcleral vessels and can be seen in Figure 7. Rattlesnaking may be caused by a number of factors such as nearby vessels, variations in scattering properties of background tissue, and groups of erythrocytes flowing in vessels. In small vessels, rattlesnaking may be enhanced in magnitude by the small numbers of red blood cells flowing through narrow vessels.

In this study, only the short-term repeatability of oximetry measurements was assessed. In future, quantification of repeatability of measurements over the course of an entire day is desirable to assess longer term variations including fluctuating diurnal variation in vessel diameter and temperature of bulbar conjunctival vessels (Duench et al., 2007).

4.5. Influence of light scattering by scleral tissue

Optical scattering of light by tissue may influence ODR and vessel diameter measurement. We assume negligible scattering for the bulbar conjunctival vasculature, which lies within a thin (~33μm), transparent bulbar conjunctiva (Efron et al., 2009). However, episcleral vessels are embedded in scleral tissue; this will affect our measurement in two ways. Firstly, the sharpness of vessel boundaries may be decreased, which may produce a small increase systematic and random errors in the measurement of vessel diameter for episcleral vessels. The relative change in vessel diameter measured will however be relatively unaffected by scattering. Secondly, scattering from overlying tissue will act to reduce contrast of vessels, generally acting to reduce the changes in ODR observed. Secondly, scattering from overlying tissue will act to reduce contrast of vessels, generally acting to reduce the changes in ODR observed. Scattering will also be increased if

vessels dilate; this will reduce the apparent change in ODR of episcleral vessels which were observed to dilate significantly (see Figure 6e). In the scleral phantom, the FEP plastic of the capillary will contribute to scattering. The challenge of light scattering by tissue and within blood and the absence of reliable SO_2 values for calibration, makes absolute oximetry in bulbar conjunctival and episcleral vessels challenging, however, as we describe here, changes in SO_2 can be robustly characterised with ODR and can provide useful biological insight.

4.6. Future work

There are good prospects of achieving an absolute oximetry, with minimal requirement for calibration by incorporating the modified Beer-Lambert law (Delpy et al., 1988; Pittman and Duling, 1975) into multi-waveband optical transmission models. Absolute oximetry would be of particular use because there have been no reference values for SO_2 of the bulbar conjunctival or episcleral microvasculature reported in the literature, so two wavelength oximetry cannot be accurately calibrated.

With appropriate flash illumination, imaging at 100Hz or greater could be achieved and oximetry in smaller bulbar conjunctival vessels and capillaries could be enabled by adapting a slit lamp for high-magnification multispectral imaging. This could enable the potential for non-contact oximetry of groups of red blood cells in humans in vivo. Individual red blood cell oximetry has previously been achieved ex vivo using SMSI (Fernandez Ramos et al., 2014) and invasively in vivo in anaesthetised mice by photoacoustic microscopy (Wang et al., 2013). SMSI offers faster image acquisition and a simpler image system compared to PAM.

4.7. Vascular conditions that may affect anterior segment vessel SO_2

Understanding SO_2 of bulbar conjunctival and episcleral vessels may provide insight into a range of conditions. For example, diabetic retinopathy is known to result in increased retinal vessel SO_2 (Hammer et al., 2009; Hardarson and Stefánsson, 2012), however, previous studies have shown that oxygen tension in diabetic subjects is lower than in healthy controls (Isenberg et al., 1986). Further, diabetes is associated with increased bulbar conjunctival vessel diameter (Cheung, Anthony T. W. Ramanujam et al., 2001), capillary loss (Owen et al., 2008), and decreased vessel reactivity (Fenton et al., 1979). Snapshot multispectral-imaging oximetry could also provide direct in vivo measurement of resultant hypoxia in bulbar conjunctival vasculature from contact lens wear (Heitmar et al., 2012; Sweeney, 2013). Furthermore oximetry of the bulbar conjunctival vessels may be of interest in studying the recovery of ocular burns using oxygen therapy (Sharifipour et al., 2011), recovery of circulation after surgical or traumatic wound healing, and possibly in the study of ischemic conditions such as dry-eye syndrome (Menezo and Lightman, 2004). High intra-ocular pressure (IOP) is associated with narrowed episcleral veins and increased diameter of episcleral arteries (Nanba and Schwartz, 1986), but it is not known if this may alter episcleral SO_2.

5. Conclusions

This is the first study to quantify changes localised in SO_2 of bulbar conjunctival and episcleral microvasculature. Oximetry was achieved using SMSI and was validated using a sclera-mimicking phantom.

In vivo, acute mild hypoxia resulted in a repeatable reduction in SO_2 of both bulbar conjunctival and episcleral microvasculature. Episcleral vessels were observed to dilate due to acute mild hypoxia, whereas bulbar conjunctival vessels did not show

statically significant dilation under hypoxia. Hypoxic bulbar conjunctival vessels were observed to rapidly reoxygenate due to oxygen diffusion when exposed to ambient air. Episcleral vessels were not observed to reoxygenate due to overlying episcleral tissue. This oxygen diffusion means that after exposure to air, the pO_2 of bulbar conjunctival vessels will be in equilibrium with ambient air, resulting in a SO_2 close to 100%. SMSI is currently the only oximetry technique with sufficient spatiotemporal resolution to measure this rapid oxygen diffusion in individual vessels. However we have shown that the role of oxygen diffusion in the bulbar conjunctiva must be considered for any future oximetry studies to provide meaningful results.

SMSI oximetry of the bulbar conjunctival and episcleral microvasculature may be of interest in investigating oxygen dynamics in a variety of microvasculature conditions where hypoxia may play a role, such as diabetes, (Isenberg et al., 1986; Hammer et al., 2009; Hardarson and Stefánsson, 2012), sickle-cell disease (Isenberg et al., 1987), dry-eye syndrome (Menezo and Lightman, 2004), contact lens wear (Heitmar et al., 2012; Sweeney, 2013), high intra-ocular pressure (Nanba and Schwartz, 1986), traumatic or surgical wound healing, and ocular-burn recovery (Sharifipour et al., 2011). Further, high-magnification MSI of the bulbar conjunctiva could enable non-invasive in vivo oximetry of individual red blood cells.

References

Alabboud, I., Muyo, G., Gorman, A., Mordant, D., McNaught, A., Petres, C., Petillot, Y.R., Harvey, A.R., 2007. New spectral imaging techniques for blood oximetry in the retina. Proc. SPIE 6631, Nov. Opt. Instrum. Biomed. Appl. III 6631. doi:10.1117/12.728535

Bashkatov, A.N., Genina, E.A., Kochubey, V.I., Tuchin, V. V., 2010. Optical

properties of human sclera in spectral range 370-2500 nm. Opt. Spectrosc. 109, 197–204. doi:10.1134/S0030400X10080084

Beach, J.M., Schwenzer, K.J., Srinivas, S., Kim, D., Tiedeman, J.S., 1999. Oximetry of retinal vessels by dual-wavelength imaging: calibaration and influence of pigmentation. JAP 86, 748–758.

Boeckaert, J., Vandewalle, E., Stalmans, I., 2012. Oximetry: recent insights into retinal vasopathies and glaucoma. Bull. Soc. Belge Ophtalmol. 75–83.

Briley-Saebo, K., Bjornerud, A., 2000. Accurate de-oxygenation of ex vivo whole blood using sodium dithionite. Proc. Intl. Soc. Mag. Reson. Med 2025.

Chapman, K.R., Liu, F.L., Watson, R.M., Rebuck, A.S., 1986. Conjunctival oxygen tension and its relationship to arterial oxygen tension. J. Clin. Monit. 2, 100–104.

Cheung, A., Hu, B., Wong, S., Chow, J., Chan, M., To, W., Li, J., Ramanujam, S., Chen, P., 2012. Microvascular abnormalities in the bulbar conjunctiva of contact lens users. Clincal hemerology Microcirc. 51, 77–86. doi:10.3233/CH-2011-1513.

Cheung, Anthony T. W. Ramanujam, S., Greer, D.A., Kumagai, L.F., Aoki, T.T., 2001. Microvascular abnormalities in the bulbar conjunctiva of patients with type 2 diabetes. Endocr. Pract. 7, 358–363.

Choudhary, T.R., Ball, D., Fernandez Ramos, J., McNaught, A.I., Harvey, A.R., 2013. Assessment of acute mild hypoxia on retinal oxygen saturation using snapshot retinal oximetry. Invest. Ophthalmol. Vis. Sci. 54, 38–43. doi:10.1167/iovs.13-12624

Crihalmeanu, S., Ross, A., 2012. Multispectral scleral patterns for ocular biometric recognition. Pattern Recognit. Lett. 33, 1860–1869. doi:10.1016/j.patrec.2011.11.006

Delpy, D.T., Cope, M., van der Zee, P., Arridge, S., Wray, S., Wyatt, J., 1988. Estimation of optical pathlength through tissue from direct time of flight

609 measurement. Phys. Med. Biol. 33, 1433–1442. doi:10.1088/0031-
610 9155/33/12/008
611 Duench, S., Simpson, T., Jones, L.W., Flanagan, J.G., Fonn, D., 2007. Assessment
612 of variation in bulbar conjunctival redness, temperature, and blood flow. Optom.
613 Vis. Sci. 84, 511–556. doi:10.1097/OPX.0b013e318073c304
614 Efron, N., Al-Dossari, M., Pritchard, N., 2009. In vivo confocal microscopy of the
615 bulbar conjunctiva. Clin. Experiment. Ophthalmol. 37, 335–344.
616 doi:10.1016/j.jfma.2013.10.003
617 Eliasdottir, T.S., Bragason, D., Hardarson, S.H., Kristjansdottir, G., Stefánsson, E.,
618 2014. Venous oxygen saturation is reduced and variable in central retinal vein
619 occlusion. Graefe's Arch. Clin. Exp. Ophthalmol. doi:10.1007/s00417-014-2849-
620 2
621 Fenton, B.M., Zweifach, B.W., Worthen, D.M., 1979. Quantitative morphometry of
622 conjunctival microcirculation in diabetes mellitus. Microvasc. Res. 18, 153–166.
623 doi:10.1016/0026-2862(79)90025-6
624 Fernandez Ramos, J., Brewer, L.R., Gorman, A., Harvey, A.R., 2014. Video-rate
625 multispectral imaging: application to microscopy and macroscopy. Opt. Soc. Am.
626 doi:10.1364/COSI.2014.CW1C.3
627 Fischer, M.J.M., Uchida, S., Messlinger, K., 2010. Measurement of meningeal blood
628 vessel diameter in vivo with a plug-in for ImageJ. Microvasc. Res. 80, 258–266.
629 doi:10.1016/j.mvr.2010.04.004
630 Gartner, S., 1944. Blood vessels of the conjunctiva, studies with high speed
631 macrophotography. Arch. Ophthalmol. 32, 464–476. doi:.
632 doi:10.1001/archopht.1944.00890120044004
633 Gorman, A., Fletcher-Holmes, D.W., Harvey, A.R., 2010. Generalization of the Lyot
634 filter and its application to snapshot spectral imaging. Opt. Express 18, 5602–8.
635 doi:10.1364/OE.18.005602

636 Hammer, M., Vilser, W., Riemer, T., Liemt, F., Jentsch, S., Dawczynski, J.,
637 Schweitzer, D., 2011. Retinal venous oxygen saturation increases by flicker light
638 stimulation. Invest. Ophthalmol. Vis. Sci. 52, 274–7. doi:10.1167/iovs.10-5537
639 Hammer, M., Vilser, W., Riemer, T., Mandecka, A., Schweitzer, D., Kühn, U.,
640 Dawczynski, J., Liemt, F., Strobel, J., 2009. Diabetic patients with retinopathy
641 show increased retinal venous oxygen saturation. Graefes Arch. Clin. Exp.
642 Ophthalmol. 247, 1025–30. doi:10.1007/s00417-009-1078-6
643 Hardarson, S.H., Harris, A., Karlsson, R.A., Halldorsson, G.H., Kagemann, L.,
644 Rechtman, E., Zoega, G.M., Eysteinsson, T., Benediktsson, J.A., Thorsteinsson,
645 A., Jensen, P.K., Beach, J., Stefánsson, E., 2006. Automatic retinal oximetry.
646 Invest. Ophthalmol. Vis. Sci. 47, 5011–6. doi:10.1167/iovs.06-0039
647 Hardarson, S.H., Stefánsson, E., 2012. Retinal oxygen saturation is altered in
648 diabetic retinopathy. Br. J. Ophthalmol. 96, 560–3. doi:10.1136/bjophthalmol-
649 2011-300640
650 Harvey, A.R., Fletcher-Holmes, D.W., Gorman, A., Altenbach, K., Arlt, J., Read,
651 N.D., 2005. Spectral imaging in a shapshot. Proc. SPIE. Spectr. Imaging
652 Instrumentation, Appl. Anal. III 5694, 110–119. doi:10.1117/12.604609
653 Heitmar, R., Wright, S., Mousavi, M., Wolffsohn, J.S., 2012. Oxygen saturation
654 measurements of the limbal vasculature before and after soft contact lens wear.
655 Contact Lens Anterior Eye 35 S1, e19. doi:doi:10.1016/j.clae.2012.08.060
656 Hill, R.., Fatt, I., 1963. Oxygen depletion of a limited resovoir by human conjunctiva.
657 Lett. to Nat. doi:10.1038/2001011b0
658 Iguchi, S., Mitsubayashi, K., Uehara, T., Ogawa, M., 2005. A wearable oxygen
659 sensor for transcutaneous blood gas monitoring at the conjunctiva. Sensors
660 Actuators B Chem. 108, 733–737. doi:10.1016/j.snb.2004.12.099
661 Isenberg, S., Neumann, D., Fink, S., Rich, R., 2002. Continuous oxygen monitoring
662 of the conjunctiva in neonates. J. Perinatol. 22, 46–49.

663 doi:10.1038/sj/jp/7210602
664 Isenberg, S.J., Mcree, W.E., Jedrzynski, M., 1986. Conjunctival hypoxia in diabetes
665 mellitus. Invest. Ophthalmol. Vis. Sci. 27, 1512–1515.
666 Isenberg, S.J., McRee, W.E., Jedrzynski, M.S., Gange, S.N., Gange, S.L., 1987.
667 Effects of sickle cell anemia on conjunctival oxygen tension and temperature.
668 Arch. Intern. Med. 147, 67–69. doi:10.1016/0736-4679(87)90250-2
669 Jiang, H., Ye, Y., Cabrera, D., Lam, B.L., Rundek, T., Tao, A., Shao, Y., Wang, J.,
670 2013. Human conjunctival microvasculature assessed with a retinal function
671 imager (RFI). Microvasc. Res. 85, 134–137. doi:10.1016/j.mvr.2012.10.003
672 Jiang, H., Zhong, J., DeBuc, D.C., Tao, A., Xu, Z., Lam, B.L., Liu, C., Wang, J.,
673 2014. Functional slit lamp biomicroscopy for imaging bulbar conjunctival
674 microvasculature in contact lens wearers. Microvasc. Res. 92, 62–71.
675 doi:10.1016/j.mvr.2014.01.005
676 Kwan, M., Fatt, I., 1971. A noninvasive method of continuous arterial oxygen tension
677 estimation from measured palpebral conjunctival oxygen tension.
678 Anesthesiology 35.
679 Labsphere Inc., n.d. Optical-Grade Spectralon® Diffuse Reflectance Material
680 Specially Fabricated for Optical Components [WWW Document]. URL
681 https://www.labsphere.com/wp-content/uploads/2015/06/Spectralon-Optical-
682 Grade.pdf (accessed 11.4.15).
683 Mader, T.H., Friedl, K.E., Mohr, L.C., Bernhard, W.N., 1987. Conjunctival oxygen
684 tension at high altitude. Aviat. Space. Environ. Med. 58, 767–769.
685 Meighan, S.S., 1956. Blood vessels of the bulbar conjunctiva in man. Br. J.
686 Opthalmology 40, 513–526.
687 Menezo, V., Lightman, S., 2004. The eye in systemic vasculitis. Clin Med 4, 250–
688 254. doi:10.1016/S0140-6736(04)17554-5
689 Mordant, D.J., Al-Abboud, I., Muyo, G., Gorman, A., Harvey, A.R., McNaught, A.I.,

2014. Oxygen saturation measurements of the retinal vasculature in treated asymmetrical primary open-angle glaucoma using hyperspectral imaging. Eye (Lond). 28, 1190–200. doi:10.1038/eye.2014.169

Mordant, D.J., Al-Abboud, I., Muyo, G., Gorman, A., Sallam, A., Ritchie, P., Harvey, a R., McNaught, a I., 2011. Spectral imaging of the retina. Eye 25, 309–20. doi:10.1038/eye.2010.222

Mordant, D.J., Al-Abboud, I., Muyo, G., Gorman, A., Sallam, A., Rodmell, P., Crowe, J., Morgan, S., Ritchie, P., Harvey, A.R., McNaught, A.I., 2011. Validation of human whole blood oximetry, using a hyperspectral fundus camera with a model eye. Invest. Ophthalmol. Vis. Sci. 52, 2851–9. doi:10.1167/iovs.10-6217

Nanba, K., Schwartz, B., 1986. Increased diameter of the anterior ciliary artery with increased intraocular pressure. Arch Opthalmol 104, 1652–1655. doi:10.1001/archopht.1986.01050230090039

Olafsdottir, O.B., Hardarson, S.H., Gottfredsdottir, M.S., Harris, A., Stefánsson, E., 2011. Retinal oximetry in primary open-angle glaucoma. Invest. Ophthalmol. Vis. Sci. 52, 6409–13. doi:10.1167/iovs.10-6985

Ormerod, L.D., Fariza, E., Webb, R.H., 1995. Dynamics of external ocular blood flow studied by scanning angiographic microscopy. Eye 9, 605–614.

Owen, C.G., Newsom, R.S.B., Rudnicka, A.R., Barman, S.A., Woodward, E.G., Ellis, T.J., 2008. Diabetes and the tortuosity of vessels of the bulbar conjunctiva. Ophthalmology 115, e27–e32. doi:doi:10.1016/j.ophtha.2008.02.009

Pittman, R., Duling, B., 1975. A new method for the measurement of percent oxyhemoglobin. J. Appl. Physiol. 38.

Prahl, S., 1999. Optical absorption of hemoglobin [WWW Document]. Oregon Med. Laser Cent.

Shahidi, M., Wanek, J., Gaynes, B., Wu, T., 2010. Quantitative assessment of conjunctival microvascular circulation of the human eye. Microvasc. Res. 79,

109–13. doi:10.1016/j.mvr.2009.12.003

Sharifipour, F., Baradaran-Rafii, A., Idani, E., Zamani, M., Jabbarpoor Bonyadi, M.H., 2011. Oxygen therapy for acute ocular chemical or thermal burns: a pilot study. Am. J. Ophthalmol. 151, 823–828. doi:10.1016/j.ajo.2010.11.005

Spurling, K.J., Zammit, C., Lozewicz, S., 2011. Mains-powered hypoxic gas generation: a cost-effective and safe method to evaluate patients at risk from hypoxia during air travel. Thorax 66, 731–2. doi:10.1136/thx.2010.141655

Sweeney, D., 2013. Have silicone hydrogel lenses eliminated hypoxia? Eye Contact Lens Sci. Clin. Pract. 39, 53–60. doi:10.1097/ICL.0b013e31827c7899

van Assendelft, O.W., 1970. Spectrophotometry of haemoglobin derivatives. Van Gorcum.

van Zijderveld, R., Ince, C., Schlingemann, R.O., 2014. Orthogonal polarization spectral imaging of conjunctival microcirculation. Graefes Arch. Clin. Exp. Ophthalmol. doi:10.1007/s00417-014-2603-9

Verma, A., Roach, P., 2010. The interpretation of arterial blood gases. Aust. Prescr. 33, 124–129.

Wanek, J., Gaynes, B., Lim, J.I., Molokie, R., Shahidi, M., 2013. Human bulbar conjunctival hemodynamics in hemoglobin SS and SC disease. Am. J. Hematol. 88, 661–664. doi:10.1002/ajh.23475

Wang, L., Maslov, K., Wang, L. V, 2013. Single-cell label-free photoacoustic flowoxigraphy in vivo. Proc. Natl. Acad. Sci. U. S. A. 2013, 1–6. doi:10.1073/pnas.1215578110

Williams, A.J., 1998. Assessing and interpreting arterial blood gases and acid-base balance. Br. Med. J. 317, 1213–1216.

Acknowledgements

This work was supported by the University of Glasgow Sensors Initiative.

744 Disclosure: L.E. MacKenzie, None; T.R. Choudhary, None; A.I. McNaught, None;

745 A.R. Harvey, None.

746

Figure 1 (a) Simplified diagram showing position of bulbar conjunctival and episcleral vasculature with respect to the sclera and ambient air. **(b)** Representative image of vasculature observed when imaging the sclera. Bulbar conjunctival vessels are marked with white arrows and episcleral vessels are marked with yellow dashed diamond arrows.

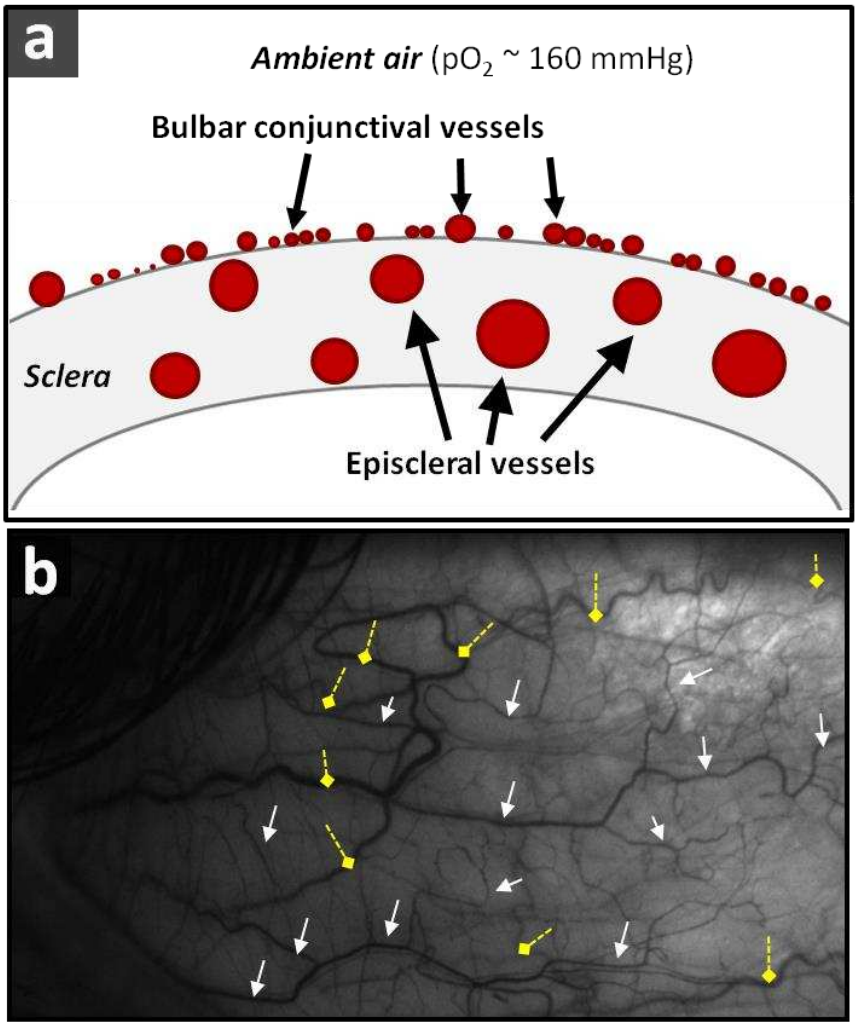

Figure 2 (a) The imaging system: a commercial fundus camera with the Image Replicating Imaging Spectrometer (IRIS) fitted to the upper imaging port. **(b)** A representative 8-band IRIS image of bulbar conjunctival and episcleral vasculature.

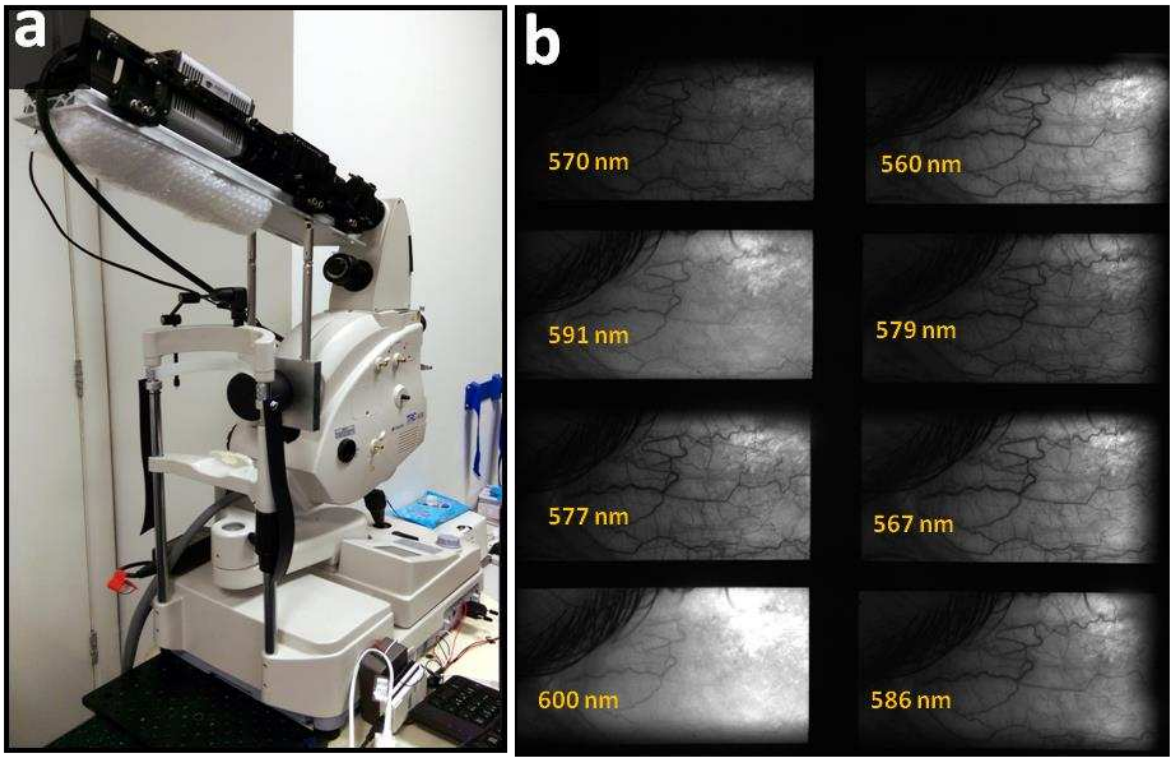

.

Figure 3. (a) diagram of the scleral phantom. **(b)** 100µm capillary filled with blood; scale bar represents one millimetre.

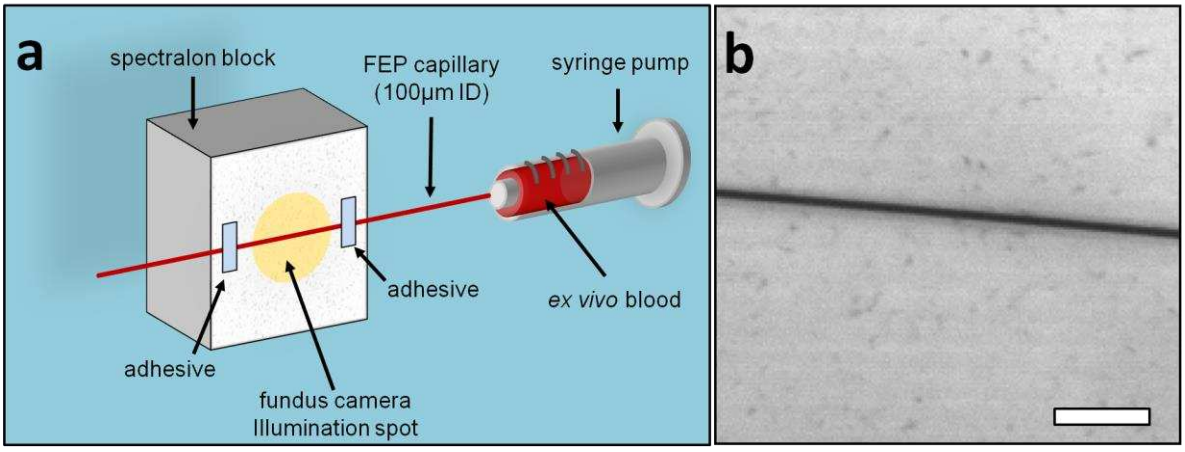

Figure 4. Depiction of the vessel fitting algorithm applied to estimate vessel diameter, the greyscale intensity in centre of vessel (I_v), and the background greyscale intensity (I_o). Vessel boundaries are defined as the points of maximum rate of change of grayscale intensity in the vessel profile.

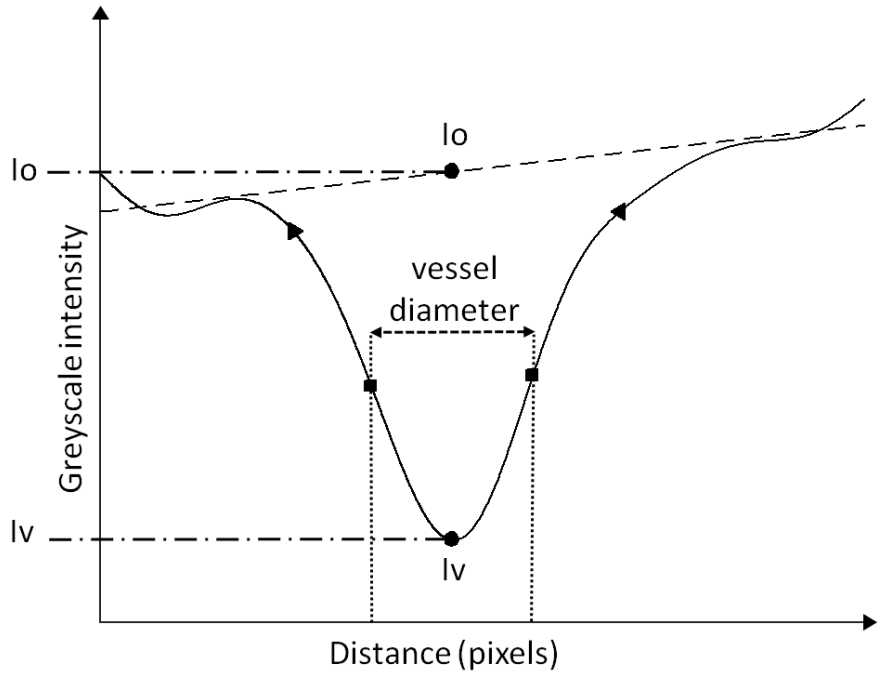

Table 1. Repeatability of optical-density ratio (ODR) measurements for conjunctival and episcleral vessels.

Parameter	Bulbar Conjunctival vessels	Episcleral vessels
Number of subjects	10	7
Total number of sampled vessel sections	57	22
ODR repeatability: individual vessels*	2.27%	2.28%
ODR repeatability**	0.96%	1.55%

*standard deviation of 8 repeated measurements of individual vessels, averaged across all subjects
** standard deviation of the average ODR of vessels when averaged by vessel type, then averaged across all subjects

Table 2. Average optical-density ratio (ODR), diameter of vessels, and pulse oximeter data at normoxia and hypoxia.

Parameter	Number of subjects	Number of vessel sections analysed	Normoxia	Hypoxia	p-value*
Conjunctival ODR (mean ± SE)	10	64	0.846 ± 0.014	0.916 ± 0.011	<0.001
Episcleral ODR (mean ± SE)	7	24	0.880 ± 0.019	0.938 ± 0.018	0.03
Conjunctival diameter (µm) (mean ± SD)	10	64	80.1 ± 7.6	80.6 ± 7.0	0.89
Episcleral diameter (µm) (mean ± SD)	7	24	78.9 ± 8.7	97.6 ± 14.3	0.02
Fingertip pulse oximeter SO_2 (%) (mean ± SD)	10	N/A	97.1 ± 1.7	86.7 ± 4.3	<0.001

*Pairwise t-test

SE = standard error

SD = standard deviation

Figure 5. Phantom validation; optical-density ratio (ODR) was measured to be inversley proportional to SO_2 as measured by a blood gas analyser (BGA). Vertical error bars represent standard deviation of ODR as measured along the length of the FEP capillary, horizontal error bars represent the blood gas anlayser manufacturers quoted error of ± 1.8% SO_2. Dashed line is fitted linear trend (R^2 = 0.89).

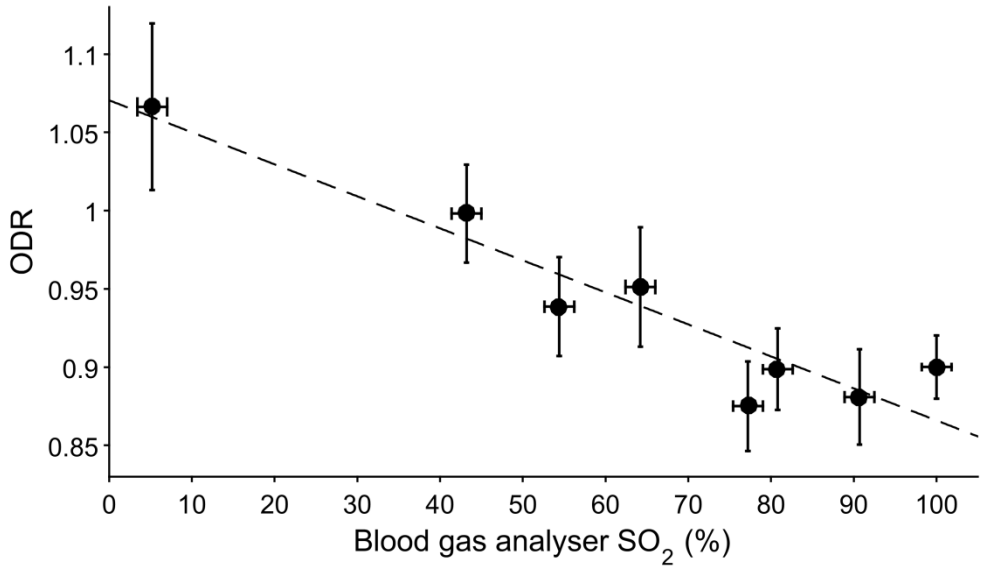

Figure 6. (a) Average optical-density ratio (ODR) and pulse oximeter data throughout the normoxia/hypoxia sequence. Error bars are the standard error of the mean. Graphs **(b)-(e)** show pairwise change of average vessel diameter and average ODR for each subject at normoxia and hypoxia. Statistically significant results are denoted with an asterix (*).

806

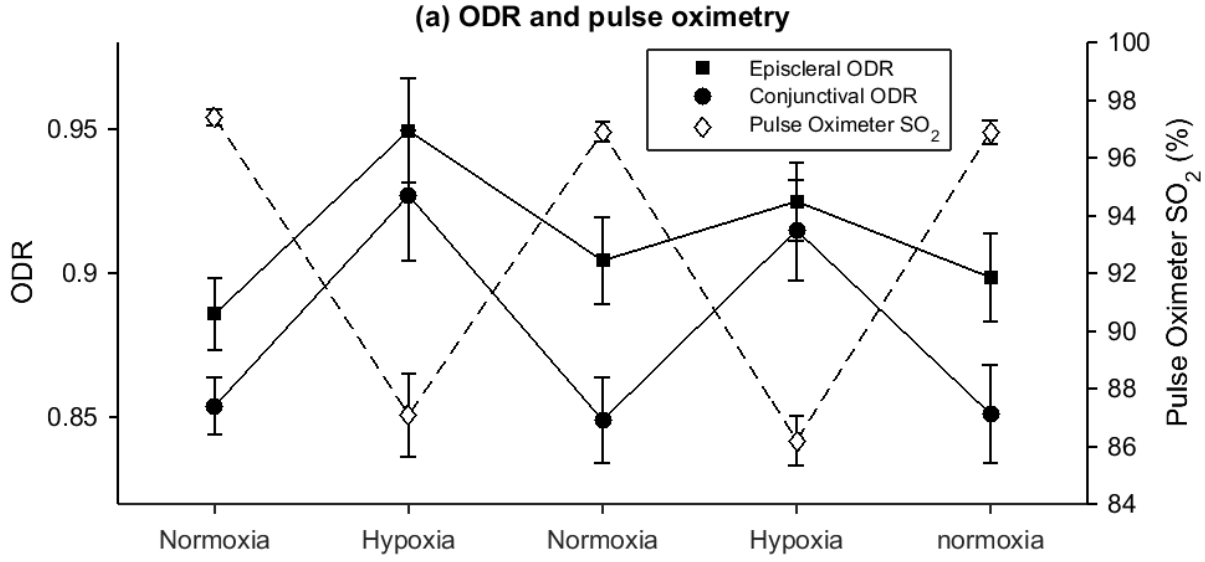
(a) ODR and pulse oximetry
Episcleral ODR
Conjunctival ODR
Pulse Oximeter SO2
ODR
Pulse Oximeter SO2 (%)
0.95
0.9
0.85
100
98
96
94
92
90
88
86
84
Normoxia
Hypoxia
Normoxia
Hypoxia
normoxia

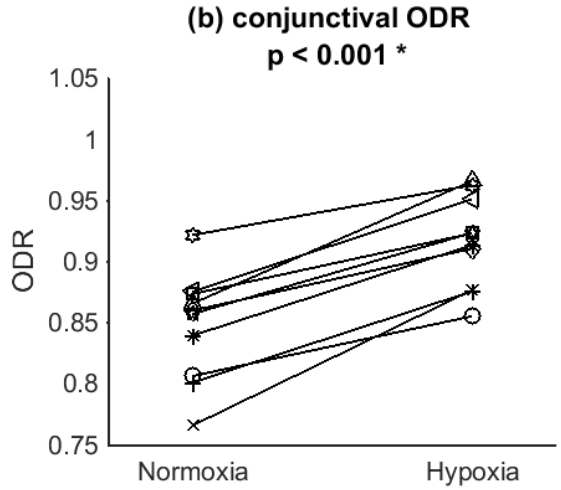
(b) conjunctival ODR
p < 0.001 *
ODR
1.05
1
0.95
0.9
0.85
0.8
0.75
Normoxia
Hypoxia

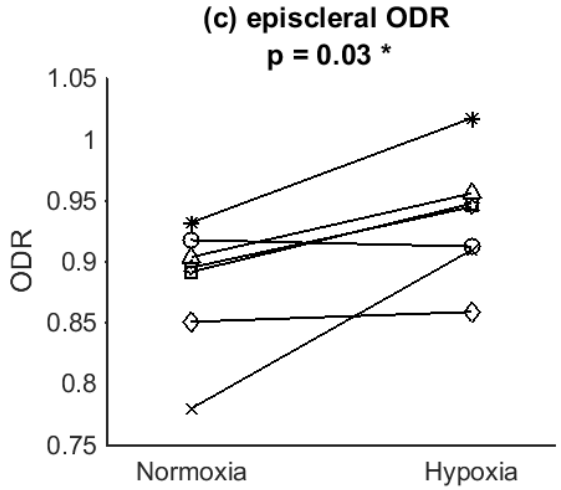
(c) episcleral ODR
p = 0.03 *
ODR
1.05
1
0.95
0.9
0.85
0.8
0.75
Normoxia
Hypoxia

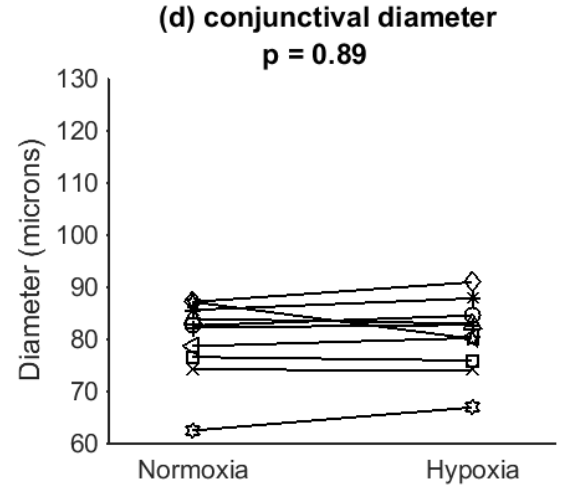
(d) conjunctival diameter
p = 0.89
Diameter (microns)
130
120
110
100
90
80
70
60
Normoxia
Hypoxia

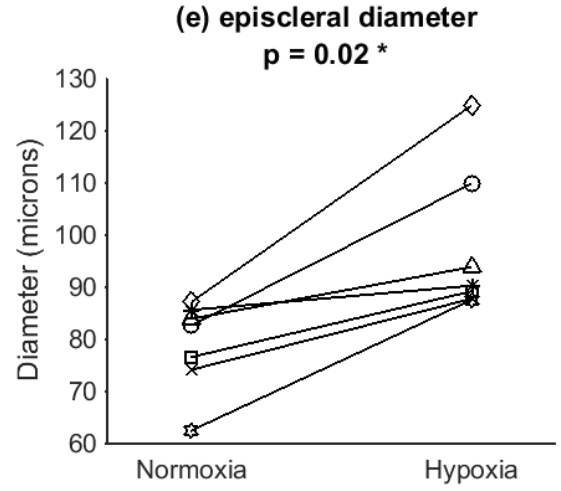
(e) episcleral diameter
p = 0.02 *
Diameter (microns)
130
120
110
100
90
80
70
60
Normoxia
Hypoxia

807
808

Figure 7. Optical-density ratio (ODR) map of vasculature at **(a)** normoxia and **(b)** hypoxia. ODR increases (i.e. SO_2 decreases) with hypoxia. Episcleral vessels are labelled with (ES) and bulbar conjunctival vessels are labelled (BC). Scale bar represents 500 µm.

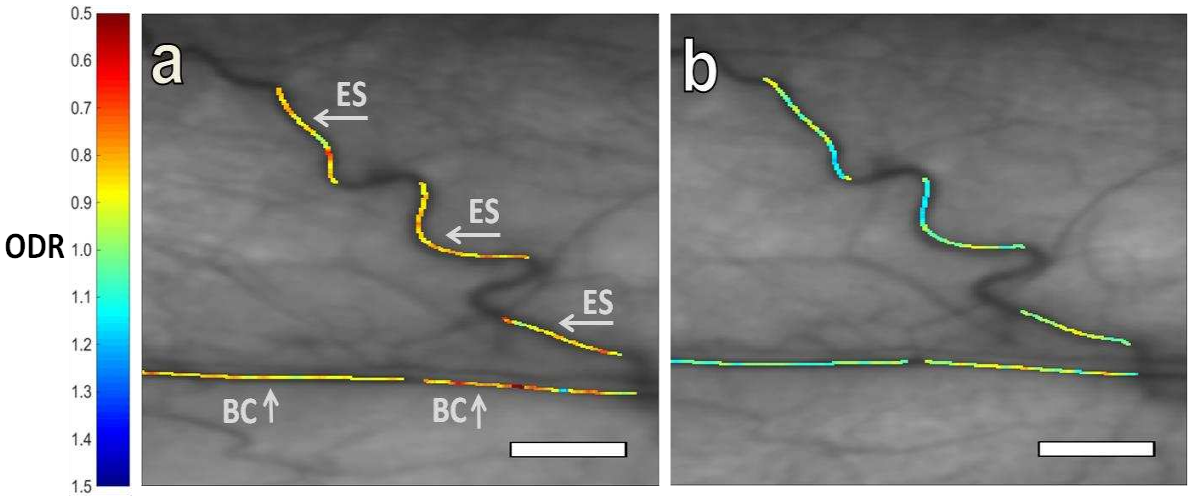

Figure 8. Optical-density ratio (ODR) of hypoxic vasculature versus time after eyelid opening (i.e. exposure to ambient air) in two representative subjects. Bulbar conjunctival ODR (blue fitted line) decreased exponentially upon eyelid opening before reaching normoxia baseline levels (blue dashed line). Episcleral ODR (red fitted line) remained higher than normoxia levels (red dashed line). This indicates that hypoxic bulbar conjunctival vessels rapidly reoxygenated by oxygen diffusion when exposed to ambient air whereas hypoxic episcleral vessels (embedded in episcleral tissue) did not reoxygenate. Error bars represent the standard error of the mean. The green fitted line is pulse oximeter data (± 2% SO_2 uncertainty quoted by the manufacturer not depicted for clarity).

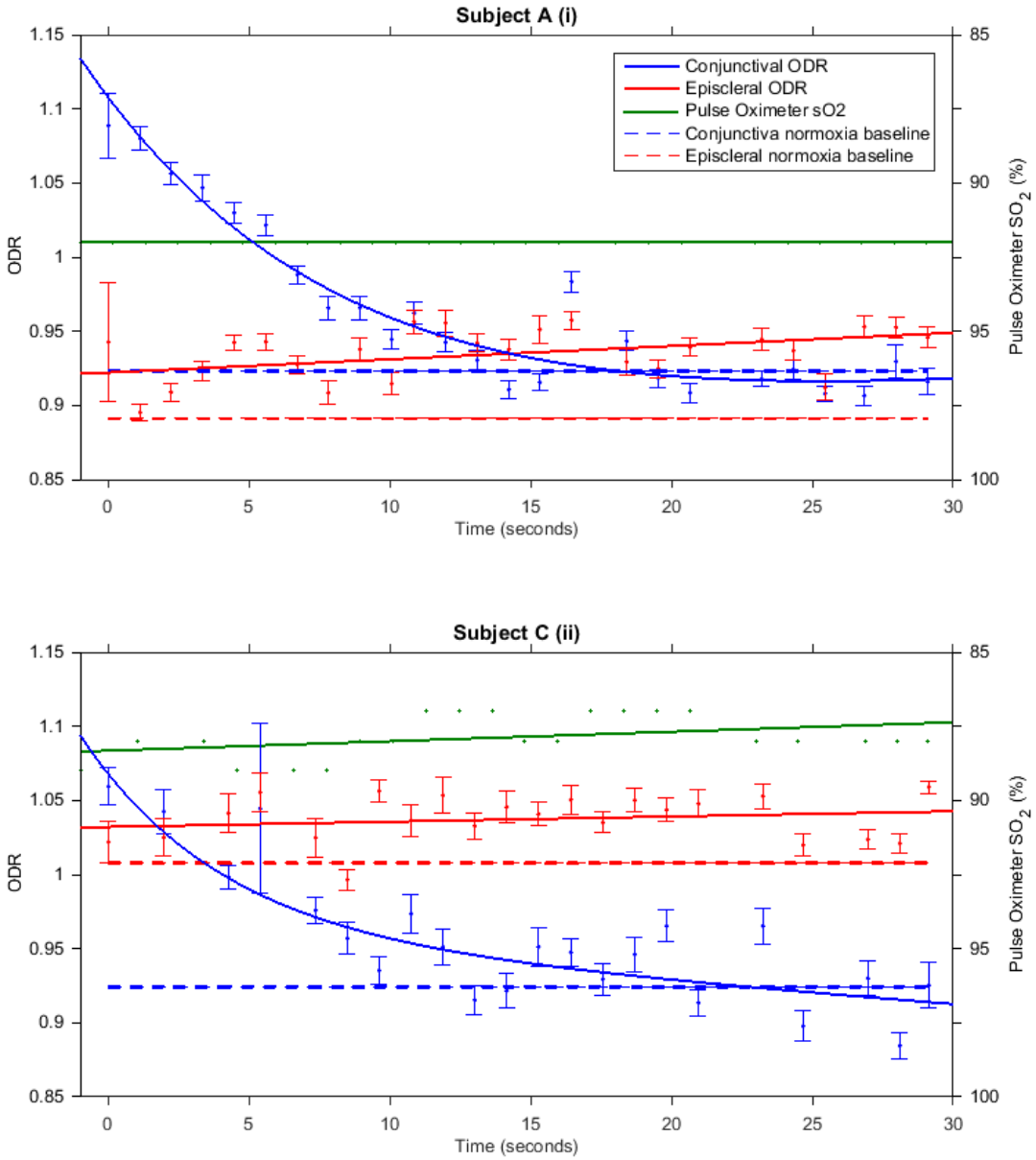

827

Table 3. Calculated values of '1/2 time to reoxygenation' ($T_{1/2}$) for 4 subjects, repeated twice per subject.

Subject	Data set	$T_{1/2}$ (seconds)
A	(i)	6.6
	(ii)	4.1
B	(i)	3.0
	(ii)	2.9
C	(i)	2.1
	(ii)	3.4
D	(i)	2.2
	(ii)	3.2
	Average	**3.4**
	Standard Deviation	**1.4**